Available online at www.sciencedirect.com
SCIENCE DIRECT
Journal of the European Ceramic Society 26 (2006) 73–80
www.elsevier.com/locate/jeurceramsoc

Preparation and sintering of nanocrystalline ITO powders with different SnO_2 content

Sung-Min Kim[a], Kyung-Han Seo[a], Joon-Hyung Lee[a], Jeong-Joo Kim[a,*], Hee Young Lee[b], Jai-Sung Lee[c]

[a] *Department of Inorganic Materials Engineering, Kyungpook National University, Daegu 702-701, Republic of Korea*
[b] *Department of Materials Science and Engineering, Yeungnam University, Gyeongsan 712-749, Republic of Korea*
[c] *Department of Metallurgy and Materials Science, Hanyang University, Ansan 425-791, Republic of Korea*

Received 3 April 2004; received in revised form 30 September 2004; accepted 8 October 2004
Available online 8 December 2004

Abstract

The effect of SnO_2 content on the sintering behavior of nanocrystalline indium tin oxide (ITO) ceramics was examined. Nanocrystalline ITO powders with different SnO_2 content from 0 to 12 at.% were prepared by a coprecipitation method. The particle size of the ITO powders was in the range of 20–26 nm. The temperature that showed maximum densification increased as the content of SnO_2 increased. Since the solubility limit of SnO_2 in In_2O_3 is known to be about 6–8 at.%, the samples with 8 and 12 at.% Sn showed second phases after sintering. Various phase development processes of the second phases were observed, i.e., In_2SnO_5, which was observed at a low temperature, decomposed into In_2O_3 and SnO_2 at over 1000 °C, then synthesized again into $In_4Sn_3O_{12}$ at over 1300 °C. The densification behavior with respect to the SnO_2 content was explained from a viewpoint of the second phase development at different sintering temperatures.

Keywords: Powders-chemical preparation; Sintering; Inclusions; Microstructure-final; ITO; SnO_2

1. Introduction

Tin doped indium oxide (or indium tin oxide: ITO) is widely used in optical devices due to high electrical conductivity and high transparency at visible light wavelengths.[1,2] Based on these characteristics, ITO films have been fabricated for a wide range of applications. When Sn^{4+} is doped in In_2O_3, the electrical conductivity increases with the Sn concentration. The increase in conductivity can be ascribed to an increase in the carrier concentration resulting from two concomitant effects. Doping by a tetravalent cation (Sn^{4+}) results in n-type doping of the lattice by providing an electron to the conduction band. For an increased conductivity, however, limited Sn doping is available because the solubility limit of Sn in In_2O_3 is about 6–8 at.%.

It is known that a full densification of the ITO target is rarely achieved.[3,4] The evaporation problem, together with undesirable features such as nonstoichiometry and wide fluctuations in composition due to loss of Sn and In at high temperatures, result in poor densification of ITO. In order to improve densification of ITO, which is a required core technique in target industry for a uniform fabrication of ITO films, various powder processing and sintering methods have been suggested. Addition of sintering additives,[5] and hot isostatic pressing (HIP) and hot pressing (HP) have been used.[6] In order to suppress evaporation, ITO samples often have been sintered in an oxygen atmosphere.[3,4] At the same time, recent research has concentrated on the preparation of homogeneous nano-sized powders, which have a high driving force of densification.[7–9] However, metastable phases often crystallize depending on the precursors.[10,11] When the metastable phases are exposed to higher temperatures, phase transformations to the stable phases have been observed.

* Corresponding author. Tel.: +82 53 950 5635; fax: +82 53 950 5645.
E-mail address: jjkim@knu.ac.kr (J.-J. Kim).

0955-2219/$ – see front matter © 2004 Elsevier Ltd. All rights reserved.
doi:10.1016/j.jeurceramsoc.2004.10.009

When Sn^{4+} is doped in In_2O_3, since doping changes the defect chemistry of In_2O_3, doping and dopant concentration are believed to affect sintering behavior of ITO. Particularly when Sn is added over the solubility limit, metastable second phases are developed. However, there has not been a detailed preceding study about the sintering behavior with that point of view in nanocrystalline ITO powders with a wide range of Sn^{4+} content above the solubility limit. Therefore, in this study, ITO powders with various levels of Sn content were synthesized by a coprecipitation method. The sintering characteristics as well as the densification behavior of the nanocrystalline ITO powders were examined.

2. Experimental

The ITO nanocrystalline powders were prepared by a coprecipitation process using starting chemicals of high purity $In(NO_3)_3{\cdot}xH_2O$ and $SnCl_4{\cdot}xH_2O$. The starting chemicals were dissolved in distilled water individually and diluted to a concentration of 2N. The mixed solution corresponding to the composition of 0, 4, 8, 12 at.% Sn^{4+} added ITO was prepared. Coprecipitation of the ITO solution was conducted at a pH of 9.5 in a continuously stirred bath by adding NH_4OH solution and the bath temperature was maintained at 15 °C. After the precipitation, the precipitates were aged for 48 h at 15 °C for a stabilization of precipitates.[11] After washing and filtering, the precipitates were dried at 85 °C for 48 h, and then calcined at 600 °C for 1 h. Powder X-ray diffraction with nickel-filtered Cu Kα radiation (MAC, M03XHF) was used for phase identification. A TEM (Hitachi H-7100) was also used for the characterization of powders. Densification behavior of the green pellets was monitored using a thermo mechanical analyzer (Rigaku, TMA 1700) with a heating rate of 5 °C/min. Sintering was carried out at 1550 °C for 1 and 16 h in air. The density of the sintered samples was determined by the Archimedes method. The microstructure of the polished cross section of the samples was observed by using a scanning electron microscope (Hitachi S-4200).

3. Results and discussion

3.1. Preparation of the nanocrystalline ITO powders and phase development as a function of the Sn content

Fig. 1 shows the TEM pictures of the precipitates prepared by a coprecipitation method: (a), (b), (c) and (d) represent the precipitates containing 0, 4, 8 and 12 at.% of Sn, respectively. The size of the precipitates does not vary much when the Sn content is changed. In respect to the morphology of precipitates, about 50 nm rectangular particles could be observed together with a few nm fine particles in (a) of 0% Sn; a decrease in the number of rectangular particles could be observed in contrast with an increase in the volume fraction of needle-like particles as more Sn is contained in (b), (c), and (d). This morphological change of particles could be attributed to the involvement of Cl^- anion, which comes about with the addition of $SnCl_4$ as a raw material.[12]

Fig. 2 shows the X-ray diffraction patterns of precipitates: (a), (b), (c) and (d) represent the X-ray diffraction patterns of the powders containing 0, 4, 8 and 12 at.% of Sn, respectively. In the case of 0 at.% Sn, it was found that the precipitate is

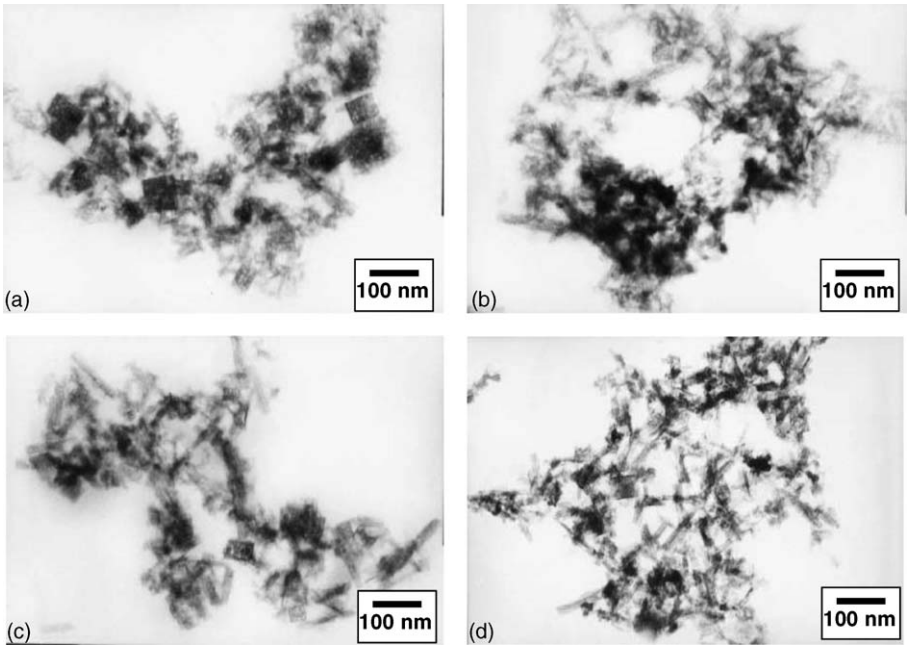

Fig. 1. TEM micrographs of In–Sn hydroxides with different Sn content of (a) 0 at.%; (b) 4 at.%; (c) 8 at.%; and (d) 12 at.%, respectively. Coprecipitation was conducted at pH 9.5, at 15 °C and aged for 48 h.

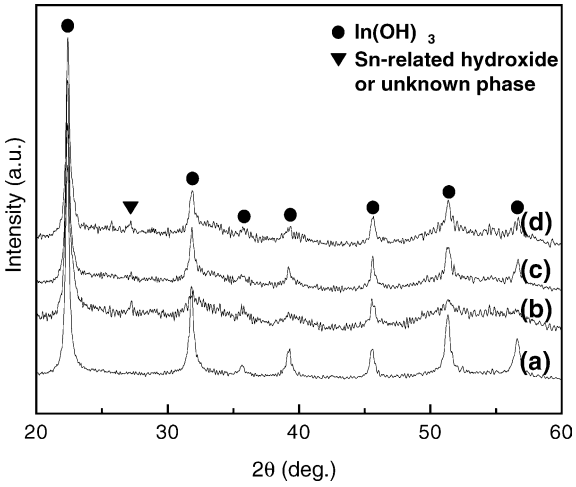

Fig. 2. X-ray diffraction patterns of In–Sn hydroxides with (a) 0 at.%; (b) 4 at.%; (c) 8 at.%; and (d) 12 at.% Sn, respectively.

Cubic $In(OH)_3$. When Sn was added there appeared a weak diffraction peak from a second phase around 27.2° as well as diffraction peaks of Cubic $In(OH)_3$. Any relevant data corresponding to the second phase, however, was hard to find from the JCPDS of In-hydrates and Sn-hydrates. Therefore, in this study it was presumed that the diffraction from the second phase is related to a mixture of In- and Sn-hydrates from the fact that the diffraction appeared in every composition containing Sn.

Fig. 3 shows the result of a thermo-gravimetry (TG) analysis of the hydrate precipitates containing 8 at.% Sn. A TG analysis was conducted in air with a heating rate of 5 °C/min.

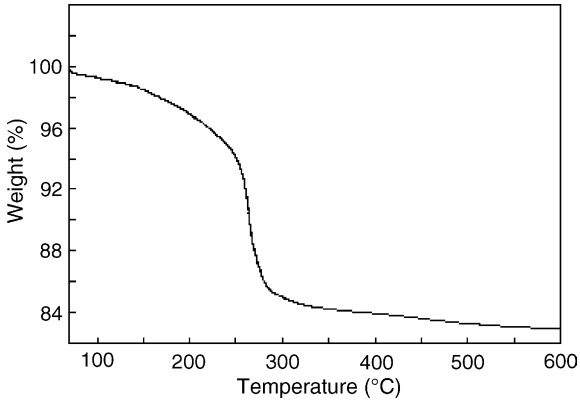

Fig. 3. TG curve of precipitates with 8 at.% Sn.

From Fig. 3 it might be certified that there is a drastic weight loss at around 260 °C and the weight loss stops at over 500 °C. Until the 500 °C mark, weight loss is estimated to be approximately 16%. This amount of loss is close to the theoretical weight loss of 16.3% by the hydration in $2In(OH)_3 \rightarrow In_2O_3 + 3H_2O(g)$. From this result, it could be confirmed that precipitates have completely turned into oxide at around 500 °C. So it was decided in the study to set the calcining temperature at 600 °C, for the sake of perfect decomposition.

The TEM pictures of nanocrystalline ITO powder acquired by calcining precipitates with a different Sn content for 1 h at 600 °C and the particle size measured based on the TEM pictures are represented in Fig. 4 and Table 1. From the TEM pictures it can be observed that the size of the particles

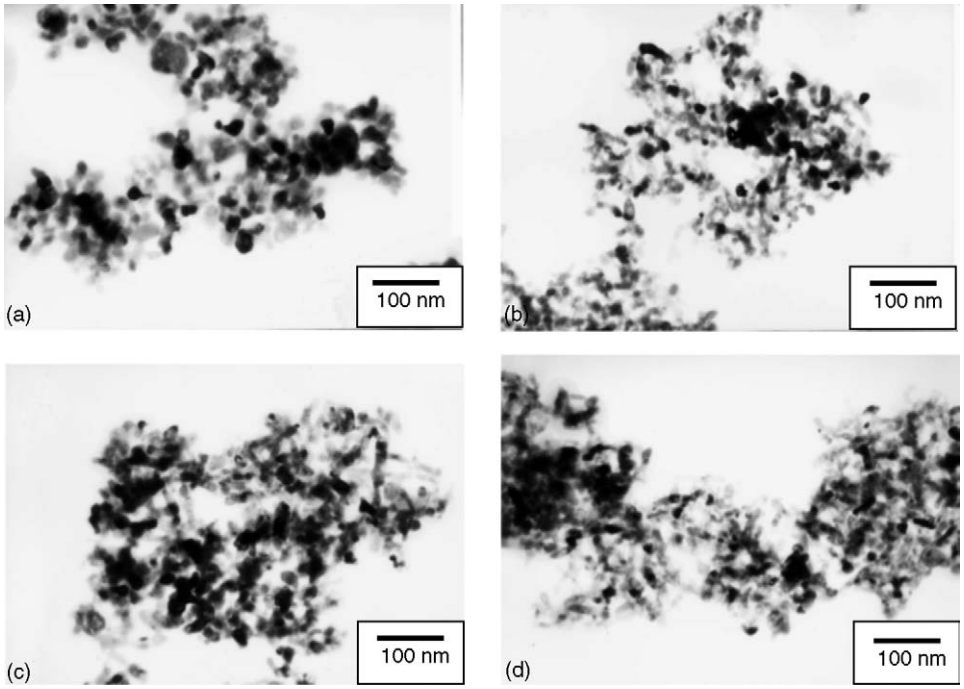

Fig. 4. TEM micrographs of ITO powders calcined at 600 °C for 1 h with (a) 0 at.%; (b) 4 at.%; (c) 8 at.%; and (d) 12 at.% Sn, respectively.

Table 1
Particle size of calcined ITO powders at 600 °C for 1 h

Sn content (at.%)	Particle size (nm)
0	26 ± 5
4	20 ± 4
8	24 ± 3
12	22 ± 4

Table 2
Phase development of ITO powders as a function of Sn content and temperature

Sn content (at.%)	600 °C	1100 °C	1350 °C
0	In_2O_3		
4	ITO		
8	ITO + In_2SnO_5	ITO + In_2O_3 + SnO_2	ITO + $In_4Sn_3O_{12}$
12			

is somewhat alike between 20 and 26 nm regardless of the Sn content. With respect to the powder shape, a spherical shape was observed in the case of 0 at.% Sn and also it was found that the aspect ratio of the needle-like particles decreased through the calcining process when Sn was included. In the case of 12 at.% Sn, however, the aspect ration of 1:3 was still maintained.

Fig. 5 shows the X-ray diffraction patterns of the powders after heat treatment for 1 h at 600, 1100, 1350 and 1550 °C as a function of the Sn content. After 48 h of aging time, a Cubic ITO phase was produced as a major phase.[13] In the composition of 4 at.% Sn only the diffraction peaks of Cubic In_2O_3[14] appeared. This can be attributed to the fact that all Sn is soluble in In_2O_3 and it forms a single phase of ITO. At the same time, various second phases such as In_2SnO_5[10] (600 °C), SnO_2 (1100 °C), $In_4Sn_3O_{12}$[15] (1350 °C and 1550 °C) were seen in the composition of 8 and 12 at.% Sn. This result indicates that the solubility limit of Sn in In_2O_3 is under 8 at.%. A summarized phase relationship with respect to the Sn content and temperature is presented in Table 2. Detail data are not presented here though, the lattice constant in the composition under 8 at.% Sn tends to increase together with an increase of the Sn content, while in the composition over 8 at.% Sn the lattice constant showed a saturated value. This result is similar to that of Nadaud et al.[16]

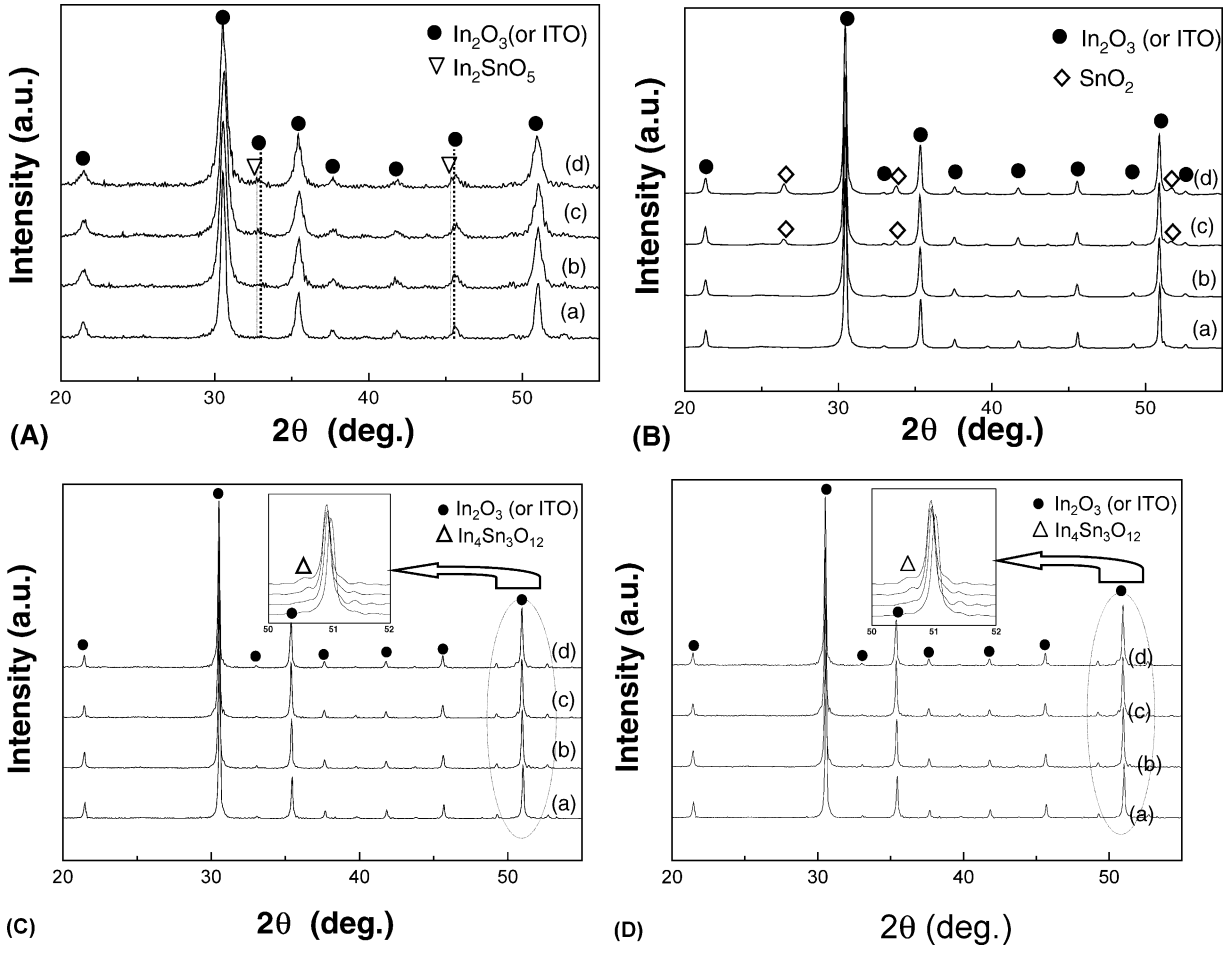

Fig. 5. X-ray diffraction patterns of ITO powders calcined at (A) 600 °C; (B) 1100 °C; (C) 1350 °C; and (D) 1550 °C for 1 h with (a) 0 at.%; (b) 4 at.%; (c) 8 at.%; and (d) 12 at.% Sn, respectively.

These authors previously explained that the solubility limit for Sn was less than 8 at.%. Considering the phase of In_2SnO_5, which neither can be observed through a general solid state reaction nor can be seen in a phase diagram, it is considered to be a metastable phase rather than a stable one. According to Varfolomeev et al.,[10] the In_2SnO_5 phase is produced when the hydroxides manufactured by the co-precipitation method such as this study are heat treated at a temperature between 600 and 700 °C and are decomposed into initial raw materials of In_2O_3 and SnO_2 at over 1000 °C.

3.2. Densification behavior of nanocrystalline ITO powders

Fig. 6 shows the result of a thermo-mechanical analysis (TMA) of nanocrystalline ITO powders. Shrinkage during sintering was measured from room temperature up to 1450 °C with a heating rate of 5 °C/min in air. Fig. 6(a) shows the relative density calculated from the linear shrinkage measured by a TMA; (b) shows the shrinkage rate of samples calculated from the linear shrinkage. In (a) it is observed that the temperature at which densification starts shifted gradually to a higher temperature as the Sn content increased; (b) also shows the increase of the temperature where the maximum shrinkage rate appeared at 720 °C (0 at.%), 1200 °C (4 at.%), 1400 °C (8 at.%) and 1410 °C (12 at.%) and the maximum shrinkage rate also increased as the Sn content increased.

The host oxide In_2O_3 is an ionic-bound semiconducting oxide (space group *Ia*3). During its formation, point defects are formed relatively easily compared with covalently bonded materials. The defects consist mainly of oxygen vacancies, giving rise to free electrons. Therefore this material has an n-type character. ITO has an anion-deficient fluorite derivative cubic structure (bixbyite structure) in which there are two non-equivalent indium sites, one where the oxygens are positioned at the corners of a slightly distorted cube with two body-diagonal sites unoccupied, and the other where the oxygens are positioned at the corners of a different distorted cube with two face-diagonal sites unoccupied.[15] This means that ITO has originally vacant oxygen sites in the bixbyite structure of In_2O_3, which corresponds to the 16c site in the space group of *Ia*3.[17] Therefore, the major defect in ITO is the originally formed inherent oxygen vacancy.[18] In the bixbyite structure, the inherent oxygen vacancy plays an important role in diffusion particularly for cations of In and Sn because the oxygen empty sites play a role of diffusion channels. According to the previous studies,[16,18,19] it was reported that the carrier concentration or conductivity became more or less independent beyond a critical Sn content. The experimental results were explained due to the formation of electrically inactive (neutral) $2Sn_{In}^{\bullet}O_i''$ association,

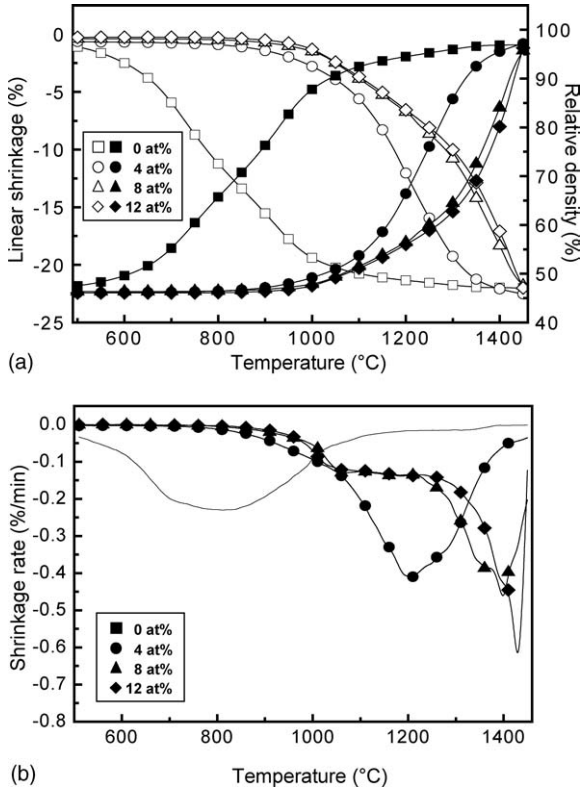

Fig. 6. Linear shrinkage and relative density of ITO specimens as a function of the Sn content: (a) the relative density is calculated from the linear shrinkage; (b) shrinkage rate of the ITO ceramics calculated from the linear shrinkage.

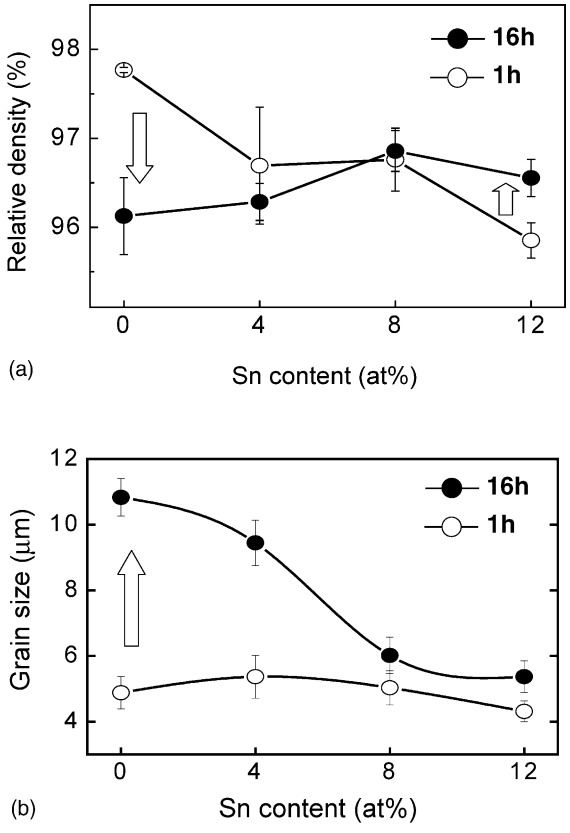

Fig. 7. (a) Relative density and (b) grain size of ITO samples sintered at 1550 °C as functions of Sn content and sintering time.

in which two electrons are trapped by an interstitial oxygen O_i'' that fills up the inherent oxygen vacancy in the bixbyite structure. From this point of view, when Sn is substituted to the In sites, the defect model considering mass conservation becomes $[Sn_{tot}] = [Sn_{In}^{\bullet}] + 2[(2Sn_{In}^{\bullet}O_i'')^x]$ As the dopant level of Sn increased the concentration of oxygen interstitial increased. In this case, it is believed that the diffusivity of ions is suppressed because the oxygen interstitials obstruct atomic movement which in return retards densification. Over the solubility limit at around 8 at.% Sn, the second phases as well as oxygen interstitials simultaneously affect the densification.

On the other hand, in the shrinkage rate graph of Fig. 6(b) it is represented that the densification proceeded through a single and continuous shrinkage process in the case of 4 at.% Sn, while the shrinkage rate was consistently maintained between 1020 and 1300 °C in the case of 8 and 12 at.% Sn. The plateau shrinkage rate between 1020 and 1300 °C was observed in the composition of 8 and 12 at.% Sn, and it is related

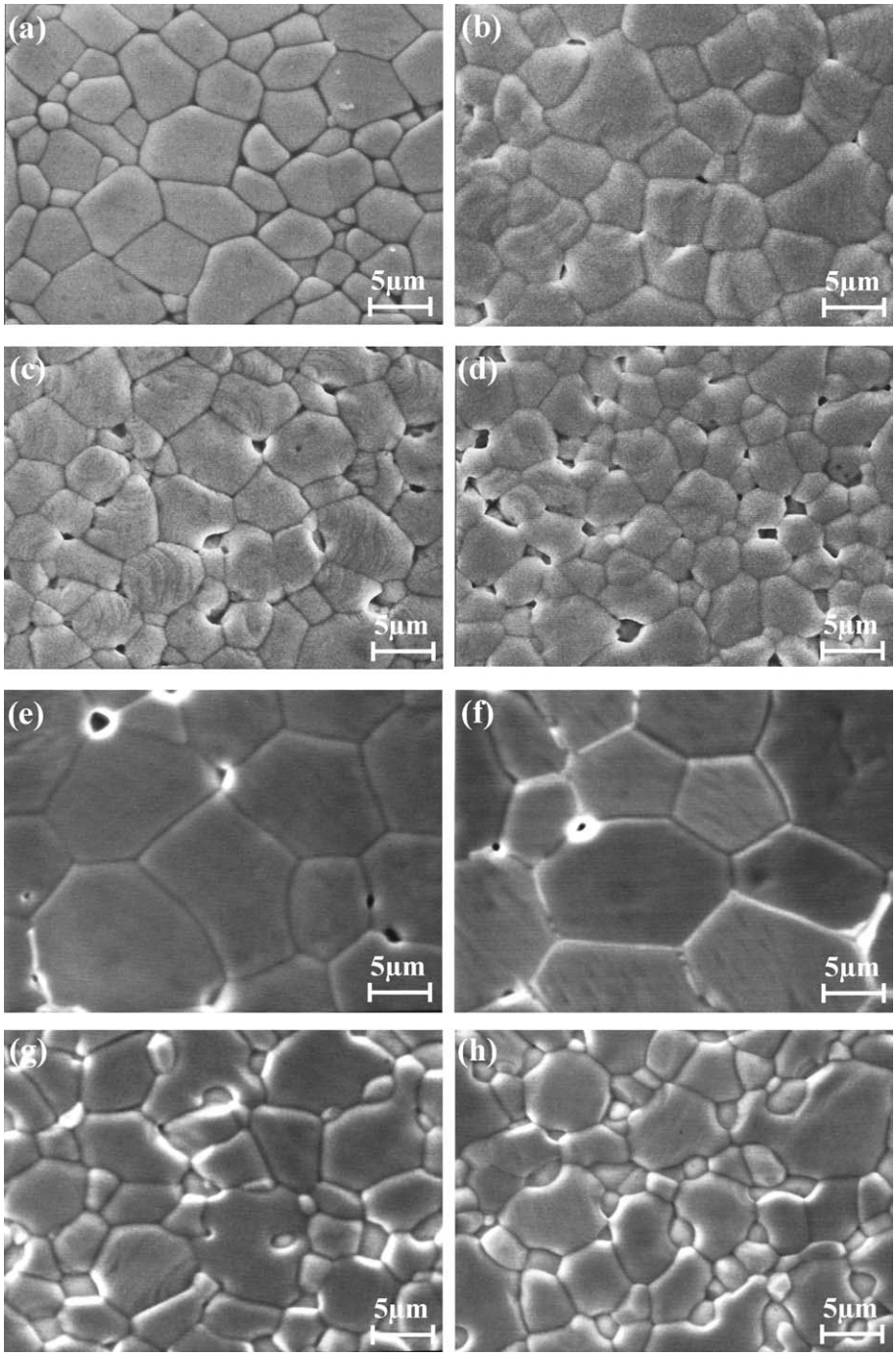

Fig. 8. SEM micrographs of ITO ceramics sintered at 1550 °C for 1 h with (a) 0 at.%; (b) 4 at.%; (c) 8 at.%; and (d) 12 at.% Sn, and sintered for 16 h with (e) 0 at.%; (f) 4 at.%; (g) 8 at.%; and (h) 12 at.% Sn.

to the metastable second phase of In_2SnO_5. In other words, it seems that the shrinkage rate is retarded as the volume fraction of the second phase at the grain boundary increased by the decomposition of In_2SnO_5 into the phases of In_2O_3 and SnO_2 at over 1000 °C. Regarding the re-increase of the shrinkage rate at over 1300 °C, it is due to the decrease of the volume fraction of the second phases at the grain boundary, while the phases of In_2O_3 and SnO_2 are synthesized again into $In_4Sn_3O_{12}$. Upon the phase transformation, because the sum of the molar volume of In_2O_3 and SnO_2 is larger than that of $In_4Sn_3O_{12}$ phase by 3.4%, production of the $In_4Sn_3O_{12}$ phase contributed to the acceleration of shrinkage rate.

Fig. 7(a) shows the relative density and (b) the mean grain size which changed depending on the Sn content of ITO sintered at 1550 °C for 1 and 16 h, respectively. In the case of the composition under 4 at.% Sn, a typical phenomenon of over firing – large grain growth and the decrease of apparent density – was observed as the sintering time was extended from 1 to 16 h. When grains grow by prolonged sintering time such as 16 h, pores at the grain boundaries can coalesce, which lead to a porosity increase owing to the decrease of capillary pressure around the pores.[20,21] Therefore, pore coalescence by grain growth can lead to density decrease. In the case of the composition over 8 at.% Sn, however, there was little grain growth while the apparent density was increased significantly.

Fig. 8 shows the microstructure of samples sintered at 1550 °C for 1 and 16 h in air as a function of the Sn content. In the samples of 0 and 4 at.% Sn, large grains were homogeneously distributed. On the contrary, in the samples of 8 and 12 at.% Sn it was found that the size of grains was relatively small and numerous small grains existed near grain boundaries. The numbers of the small grains increased as more Sn was included.

In order to analyze the composition of the small grains near grain boundaries, an EDS analysis was carried out. Fig. 9 represents the EDS analysis of a sintered sample with 12 at.% Sn. Compared with the surrounding grains, even though it is hard to differentiate the second phases and small ITO grains, some of the small grains showed a decreased In concentration and an increased Sn concentration at the same time, which can be concluded that the small grains near the grain boundary are the second phase of $In_4Sn_3O_{12}$. This second phase is thought to play a major role in grain growth inhibition.

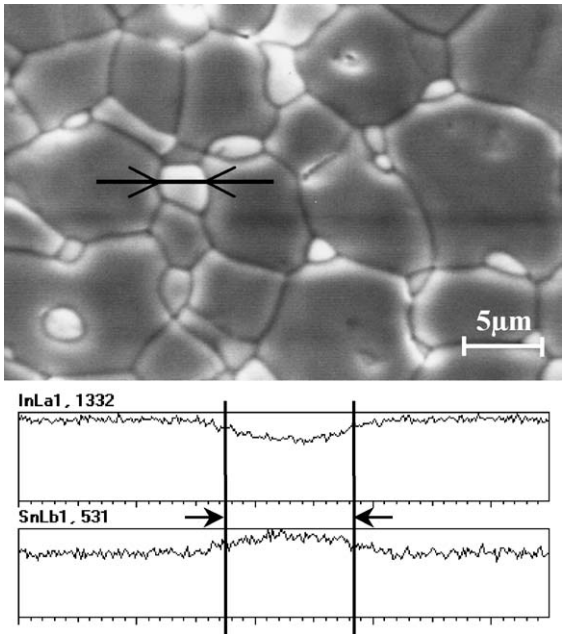

Fig. 9. EDS line scanning across a precipitate in a sample with 12 at.% Sn sintered at 1550 °C for 16 h.

4. Conclusion

The size of the nanocrystalline ITO powder prepared by a coprecipitation method is 20–26 nm regardless of the Sn content. In the case of 0 at.% Sn the powder is round-shaped while it has a high aspect ratio as more Sn is included. This shows that the morphology of the particles is somewhat Sn content dependent. The temperature at which shrinkage occurs increases as more Sn is contained. The densification is completed through a single and continuous sintering shrinkage in the cases of In_2O_3 and the composition of 4 at.% Sn, which is within the solubility limit. In the case of 8 and 12 at.% Sn which is over the solubility limit, however, the shrinkage rate is consistently maintained between 1020 and 1300 °C because the metastable second phase of In_2SnO_5 is decomposed into In_2O_3 and SnO_2. In the examination of the grain growth of the sintered sample as a function of sintering time at 1550 °C, the compositions of 0 and 4 at.% Sn showed a density reduction caused by grain growth over a long time of sintering, while compositions over the solubility limit such as 8 and 12 at.% Sn showed an increase of sintering density rather than grain growth. This is because grain growth is inhibited by the precipitation of the second phase which is thought to be $In_4Sn_3O_{12}$.

Acknowledgements

This work was supported by the Korea Research Foundation Grant (KRF-2002-002-D00092).

References

1. Hamberg, I. and Granqivst, C. G., Evaporated Sn-doped In_2O_3 films: basic optical properties and applications to energy-efficient windows. *J. Appl. Phys.*, 1986, **60**, R123–R160.
2. Cox, P. A., Flavell, W. R. and Egdell, R. G., Solid-state and surface chemistry of Sn-doped In_2O_3 ceramics. *J. Solid State Chem.*, 1987, **68**, 340–350.
3. Nadaud, N., Nanot, M. and Boch, P., Sintering and electrical properties of titania- and zirconia-containing In_2O_3–SnO_2 (ITO) ceramics. *J. Am. Ceram. Soc.*, 1994, **77**, 843–846.

4. Vojnovich, T. and Bratton, R. J., Impurity effects on sintering and electrical resistivity of indium oxide. *Am. Ceram. Soc. Bull.*, 1975, **54**, 216–217.
5. Suzuki, M., Muraoka, M., Sawada, Y. and Matsushita, J., Sintering of indium-tin-oxide with vanadium oxide additive. *Mater. Sci. Eng. B*, 1998, **54**, 46–50.
6. Martin, S., Matrin, K., Wolfgang, D. and Gruce, G., *Process for production of partially reduced indium oxide-tin oxide targets*. U.S. Patent 553,1948, 1996.
7. Nagashima, S., Yoshida, T. and Kato, A., Synthesis of In_2O_3–SnO_2 composite powders by a homogeneous precipitation technique and their sintering behavior. *Mater. Lett.*, 1994, **19**, 171–176.
8. Iwasa, K., Isobe, T. and Senna, M., Enhanced densification of indium-tin oxide ceramics for sputter target through wet mechanochemical processing. *Solid State Ionics*, 1997, **101–103**, 71–78.
9. Yura, K. and Matijevic, E., Preparation and properties of uniform coated colloidal particles. VII. Hafnium oxide on indium oxide. *J. Colloid Interface Sci.*, 1993, **153**, 328–333.
10. Varfolomeev, M. B., Mironova, A. S., Chibirova, F. K. and Plyushchev, V. E., Interaction of indium sesquioxide with stannic oxide. *Inorg. Mater.*, 1975, **11**, 1926–1928.
11. Lee, J.-H. and Chiang, Y.-M., Pyrochlore-perovskite phase transformation in highly homogeneous (Pb, La)(Zr, Sn, Ti)O_3 powders. *J. Mater. Chem.*, 1999, **9**(12), 3107–3111.
12. Kim, B. C., Kim, S. M., Lee, J. H. and Kim, J. J., Effect of phase transformation on the densification of coprecipitated nanocrystalline ITO powders. *J. Am. Ceram. Soc.*, 2002, **85**, 2083–2088.
13. Hong, D. Y., *Morphology control of $In_2O_3$and ITO powders through the coprecipitation process*. Thesis for the Degree of Master of Engineering, Seoul National University, Korea, 1996.
14. JCPDS Card Number 06-0416, International Center for Diffraction Data, 1994.
15. Minami, T., Takeda, Y., Takata, S. and Kakumu, T., Preparation of transparent conducting $In_4Sn_3O_{12}$ thin films by DC magnetron sputtering. *Thin Solid Films*, 1997, **13–18**, 308–309.
16. Nadaud, N., Lequeux, N., Nanot, M., Jove, J. and Roisnel, T., Structural studies of tin-doped indium oxide (ITO) and $In_4Sn_3O_{12}$. *J. Solid State Chem.*, 1998, **135**, 140–148.
17. Marezio, M., Refinement of the crystal structure of In_2O_3 at two wavelengths. *Acta Cryst.*, 1966, **20**, 723–728.
18. Hwang, J. H., Edwards, D. D., Kammler, D. R. and Mason, T. O., Point defects and electrical properties of Sn-doped In-based transparent conducting oxides. *Solid State Ionics*, 2000, **129**, 135–144.
19. Omata, T., Fujiwara, H., Otsuka-Yao-Matsuo, S. and Ono, N., Electron trapping center and SnO_2-doping mechanism of indium tin oxide. *Appl. Phys. A*, 2000, **71**, 609–614.
20. Kang, S. J. and Yoon, K. J., Densification of ceramics containing entrapped gases. *J. Eur. Ceram. Soc.*, 1989, **5**, 135–139.
21. Oh, U. C., Chung, Y. S., Kim, D. Y. and Yoon, D. Y., Effect of grain growth on pore coalescence during the liquid-phase sintering of MgO–$CaMgSiO_4$ systems. *J. Am. Ceram. Soc.*, 1988, **71**, 854–857.